2. Scientific Objectives

MIMI science objectives may be summarized as follows:

Saturn

- Determine the global configuration and dynamics of hot plasma in the magnetosphere of Saturn through energetic neutral particle imaging of ring current, radiation belts, and neutral clouds.
- Study the sources of plasmas and energetic ions through in situ measurements of energetic ion composition, spectra, charge state, and angular distributions.
- Search for, monitor, and analyze magnetospheric substorm-like activity at Saturn.
- Determine through the imaging and composition studies the magnetosphere–satellite interactions at Saturn and understand the formation of clouds of neutral hydrogen, nitrogen, and water products.
- Investigate the modification of satellite surfaces and atmospheres through plasma and radiation bombardment.
- Study Titan's cometary interaction with Saturn's magnetosphere (and the solar wind) via high-resolution imaging and in situ ion and electron measurements.
- Measure the high energy (E_e > 1 MeV, E_p > 15 MeV) particle component in the inner (L < 5 R_S) magnetosphere to assess cosmic ray albedo neutron decay (CRAND) source characteristics.
- Investigate the absorption of energetic ions and electrons by the satellites and rings in order to determine particle losses and diffusion processes within the magnetosphere.
- Study magnetosphere–ionosphere coupling through remote sensing of aurora and in situ measurements of precipitating energetic ions and electrons.

Jupiter

- Study ring current(s), plasma sheet, and neutral clouds in the magnetosphere and magnetotail of Jupiter during Cassini flyby, using global imaging and in situ measurements.

Interplanetary

- Determine elemental and isotopic composition of local interstellar medium through measurements of interstellar pickup ions.
- Study the compositional evolution at low energies of shock-accelerated ions in the interplanetary medium.
- Monitor cosmic ray intensity variations (E_p > 70 MeV/nuc) and anomalous cosmic rays, and compare with similar measurement in both the inner heliosphere (Advanced Composition Explorer, ACE) and the outer heliosphere (Voyager 1, 2).

2.1 Global Imaging

The most fundamental relationship in physics is that of cause and effect, and the study of the magnetospheres of the giant planets has been a valiant struggle with the inseparability of temporal and spatial variations along the flyby trajectories of Pioneers 10/11, Voyagers 1/2, and Ulysses. The exciting new observations from the Galileo orbiter are adding another dimension to our understanding, just as the Cassini orbiter certainly will. However, the most dramatic and unambiguous signatures of magnetospheric electrodynamics will come from imaging the ion populations across the huge expanses of the Saturnian magnetosphere. The Ion and Neutral Camera (INCA) will image energetic neutral atoms (ENAs) that are produced when energetic, singly charged ions undergo charge-exchange collisions with the cold neutral gas that pervades the ion populations. Because the ENA trajectories are straight lines originating at the location of the charge-exchange collision, the counting rate in each INCA pixel of the sky is proportional to the line-of-sight integral of the ion intensity (in the direction of the spacecraft) weighted by the cold neutral densities n_i and the corresponding charge-exchange rate σ_i: $j_{ENA} = \Sigma\, \sigma_i \int ds\, n_i\, j_{ION}$. Because INCA can resolve ENA hydrogen from ENA oxygen, these two species can be analyzed separately.

Nonetheless, even with resolution of H from O, the unfolding of the ion intensities from the INCA images will probably require sophisticated minimization algorithms in which parametric models of the ion intensities (and the neutral densities) are optimized so that the difference between the measured INCA pixel rates and those predicted by the models is a minimum (in a χ-squared sense).

Energetic charge exchange neutral emissions have been detected from the magnetospheres of Earth, Jupiter, and Saturn. Table 2.1 compares the measured neutral atom source strengths near 40 keV of five planetary magnetospheres (McEntire and Mitchell, 1989). The fluxes given in Table 2.1 are integrated over the source and apply for large distances compared to the source size. The source strengths agree with theoretical expectation (e.g., Ip, 1984; Cheng, 1986; Barbosa and Eviatar, 1986; Krimigis et al., 1988).

TABLE 2.1

Measured neutral atom fluxes from planetary magnetospheres near 40 keV energy at large distance d

Earth	$\sim 100 \left(\frac{d}{R_E}\right)^{-2}$ cm^{-2} s^{-1} keV^{-1} (quiet time)
Jupiter	$\sim 440 \left(\frac{d}{R_J}\right)^{-2}$ cm^{-2} s^{-1} keV^{-1}
Saturn	$\sim 240 \left(\frac{d}{R_S}\right)^{-2}$ cm^{-2} s^{-1} keV^{-1}
Uranus	$< 12 \left(\frac{d}{R_U}\right)^{-2}$ cm^{-2} s^{-1} keV^{-1}
Neptune	$< 4 \left(\frac{d}{R_N}\right)^{-2}$ cm^{-2} s^{-1} keV^{-1}

At Earth, where ENA imaging was first developed and demonstrated, the cold neutral density takes the comparatively simple form of a nearly spherically symmetrical Chamberlin exosphere of H atoms. Not so at Saturn. Reinterpretation of the Voyager 1/2 UVS Lyman-α emission demands an H-atom distribution that is more disk-like than spherical, and moreover cannot even be axially symmetric about the planet's rotation axis (Shemansky and Hall, 1992; Ip, 1996). The presence of a large amount of H in the inner system ($r < 10\ R_S$) implies that Saturn's exosphere is a significant source, but in the outer system, Ip argued that Titan should produce significant densities of H ($10 < n_{\mathrm{H}} < 10^2$ cm^{-3}) extending up to 8 R_S. Furthermore, Ip (1997) has recomputed the original estimates of Johnson et al. (1989) for the contri-

butions of the icy moons (Enceladus, Tethys, Dione, and Rhea). He finds concentrations of O, OH, and H_2O in the range 10^2 to 10^4 cm^{-3} in the inner system (3 to 6 R_S), although they are strongly confined to the equatorial plane.

Using the early models for the neutrals distribution, we have simulated idealized ENA images for INCA in Figure 2.1. "Fish-eye" lens projections of ENA fluxes (>35 keV H) are shown for four locations of Cassini. The bright object in the three more distant images is Titan's exosphere, and the putative Titan torus would be seen through most of the orbit. The color bar is logarithmic, ranging from 1% to 100% of the brightest ENA lines in each image.

Images from 50 R_S. Figure 2.2 shows Saturn and the Titan torus as viewed from the equatorial dawn meridian; distorted dipole field lines are drawn to show compression of the magnetosphere on the front side with the magnetopause at (a) 25 R_S, and (b) 20 R_S. Panel (c) shows the accumulated counts for (a) and

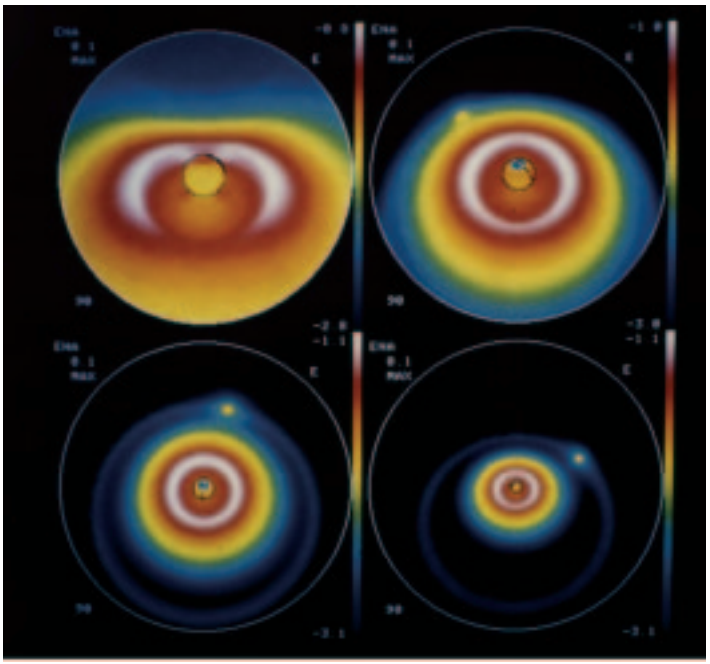

Figure 2.1. Four idealized ENA images (1° × 1° angular resolution, no Poisson statistical fluctuations in pixel counts) of the Saturn/Titan system, based on Voyager > 35 keV CPME ion measurements and early interpretation of UV observations. "Fish-eye" projection is hemisphere centered on planet (terminator indicated in black). Logarithmic color bar ranges from 1% to 100% of brightest emission in each image. Magnetosphere extends to 25 R_S, and Titan exosphere is shown with putative plasma torus. Cassini positions are every 30° of mean anomaly for inclined orbit with radius, solar longitude, magnetic latitude: (a) 4.4 R_S, 21°, 26°; (b) 5.9 R_S, 39°, 55°; (c) 9.0 R_S, 100°, 71°; and (d) 15.5 R_S, 161°, 55°.

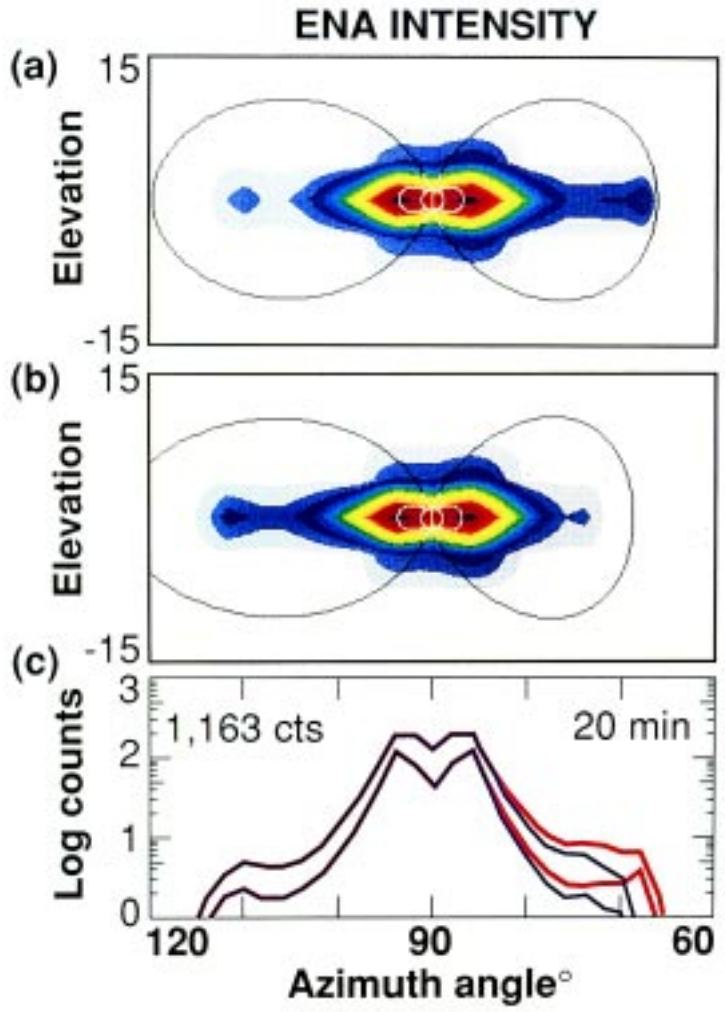

Figure 2.2. Simulated ENA images (Y = −50 R_S) of magnetopause compression from (a) 25 R_S to (b) 20 R_S detected by (c) change in Titan torus within 20 min (for 30–60 keV H).

(b) (upper and lower curves, respectively) for a 20-min accumulation. The complete image contains 1163 counts (~10% statistics in inner ring current, 30% at L = 8). Most importantly, ENA emission from the dayside Titan torus is significantly diminished as the magnetopause moves inward, thus enabling continuous remote sensing of such compressions, which is not possible through any other technique.

The implications of this complicated neutral distribution for ENA imaging can be looked at two ways. On one hand, it makes the problem of extracting absolute ion intensities from global ENA images extremely challenging. Clearly the Cassini UV

measurements of the neutral environment and the INCA ENA intensities must be correlated wherever possible. On the other hand, the concentration of the neutrals close to the equatorial plane actually simplifies the geometry for ion injection events on localized magnetic flux tubes. At Earth, ion injection events are often difficult to analyze precisely because of the spherical distribution of the H atoms—the entire flux tube "lights up" in ENA, making it hard to determine the region of L and mean local time (MLT) containing the injection. However, at Saturn, it will be mainly the equatorial region that will emit the ENA, thus giving directly the L–MLT location of the ion injection (without complicated unfolding of the line-of-sight integrals).

Consequently we anticipate that INCA, in combination with CHEMS and LEMMS, will produce immediate and quantitative identification of the regions of ion acceleration in Saturn's magnetosphere, some of which we can expect by analogy to the Earth-like ion injection events identified at Jupiter by Mauk et al. (1997) using the Galileo Energetic Particle Detector. It will be the causal relationships—what ions were accelerated where and when—that we look forward to discovering with INCA's global imaging.

2.2 Satellite Interactions and Aurora

2.2.1 *Magnetosphere–Satellite Interactions*

A major magnetospheric goal of the Cassini mission is the measurement of the environments of the Saturnian moons and the determination of their interaction with the Saturnian magnetosphere. To this end the Cassini spacecraft will conduct numerous close (<2000 km) encounters with the moons Titan, Iapetus, Hyperion, Rhea, Dione, and Enceladus. Observations from such close encounters provide the measurements required to determine the environment of the moon and its magnetospheric interaction. In particular, energetic particle measurementswith the LEMMS sensor during close flybys provide vital and often unique results that identify the character of the moon–magnetosphere interaction. For example, as has been shown at Jupiter, energetic particle observations provide a measure of the moon's surface magnetic field (Williams et al., 1997b); directly measure the effect of the moon and

its environment on the convecting magnetospheric plasma (Williams et al., 1997a); provide a direct measure of the amount of scattering occurring on planetary field lines intersecting the moon (Williams and Mauk, 1997); provide a measure of the conductivity of the moon and its environment (Paranicas et al., 1998); provide a direct measure of the effectiveness of sputtering in the formation of the moon's atmosphere, ionosphere, and associated gas torus as well as for surface mass redistribution effects (Ip et al., 1997,1998; Lagg et al. 1998); and for moons with magnetic fields can identify the existence of trapped particles within that field (Williams et al., 1997a).

On a broader scale, simultaneous observations by MIMI and the ultraviolet spectrometer will further elucidate the effects of magnetospheric interactions with Titan and the icy moons. The ultraviolet spectrometer observations will provide the H column density along the same lines of sight viewed by MIMI, enabling the energetic ion distributions to be obtained from the ENA images. The ENA images, obtained separately for each species, will allow a determination of the composition of the distant energetic ion population, thus providing a measure of the strengths of the various moons as sources of magnetospheric ions.

2.2.2 *Saturn's Aurora and Magnetospheric Activity*

Saturn's auroral energetics and morphology are Earth-like rather than Jovian, suggesting that the aurora is powered by a solar wind interaction (Sandel and Broadfoot, 1981). Alternatively, Barbosa (1987) has argued that Saturn's aurora may be powered by a Titan interaction with the magnetosphere. MIMI measurements during the many flux tube crossings at Titan will directly test this possibility. For example, at Jupiter's moon Io, intense energetic electron beams were measured flowing in both directions along Jovian field lines adjacent to Io (Williams et al., 1996). An Io flux tube full of these beams would lead to aurorae at its footprint in the Jovian atmosphere. The flux tube measurements to be made with LEMMS at Titan will yield the energy content of the particles flowing into Saturn's atmosphere and thus measure the auroral producing capability of the moon. The existence or absence of field-aligned beams at Titan will assess the effectiveness of Titan (and its environ-

ment) in converting the induced electric field resulting from its motion through the Saturnian magnetosphere into a magnetic field–aligned potential drop. Finally MIMI will search for field-aligned particle flows in the high latitude regions of Saturn's magnetosphere and directly test for the existence of field-aligned auroral zone potentials above ~10 keV. Measurements from MIMI will determine whether the resulting energetic particle precipitation is sufficient to excite aurorae.

The existence of aurorae implies the existence of substorms. At Earth the solar wind interaction with the magnetosphere provides the dominant energy source for substorms. It is not clear what the mechanism for substorm phenomena would be at Jupiter and Saturn and, until the recent systematic study of the Jovian environment by the energetic particle instrument on Galileo by Krupp et al. (1998) and by Woch et al. (1998, 1999), it was not known whether Jupiter and Saturn could be expected to display substorm phenomena. Energetic ion and electron measurements in the Jovian magnetosphere show signatures that are basically identical to substorm injection events observed at Earth (Mauk et al., 1997a). Measurements of the energy dispersion of both ions and electrons show particle injection over a narrow longitudinal band and subsequent magnetic gradient drift superimposed on magnetospheric corotation. Because of the overwhelming effect of corotation, the dispersion is best observed in the energetic particle population and is very difficult to observe at low energies. Thus, with the existence of aurorae at Saturn, it is reasonable to expect to observe substorm signatures. MIMI will provide the best opportunity to observe such signatures.

2.2.3 *Ring Interactions*

An important goal of the MIMI investigation is to understand the interactions between the planetary magnetospheric environments and Saturn's planetary rings. From the perspective of planetary ring science, charged particle environments can electrically charge ring and other particulates, thereby affecting the transport of the particulates, and perhaps of larger ring members, via collisions with the particulates (Mendis et al., 1984, Goertz, 1989). The "spokes" of Saturn are the best-known example, and the braiding of the F-ring may also have an electromagnetic origin

(Mendis et al. 1984). Energetic charged particles can modify, sputter, and erode ring particle surfaces (Johnson, 1990). In addition, charged particle distributions can provide powerful diagnostics on the presence, character, and distributions of sparse ring materials (Esposito et al., 1984, Krimigis and Armstrong, 1982). From the magnetospheric science perspective, rings provide important sources and sinks of the neutral and charged particles of planetary environments (e.g., Van Allen, 1984; Krimigis and Armstrong, 1982). Also, ring/charged-particle interaction features provide powerful diagnostics on the transport of charged particles within the magnetospheric environments (e.g., Van Allen, 1984; Mauk et al., 1994). Finally, the charged particle and ring particulate environments of planetary magnetospheres are perhaps the best laboratories for studying certain aspects and phases of the formation of planetary nebula (Burns et al., 1994).

Numerous signatures of the interaction between energetic charged particles and ring particles were observed by Pioneer 11 and the Voyagers 1 and 2. Figures 2.3 and 2.4 show, respectively, examples of explicit radial profile signatures and bite-outs in pitch angle distributions attributed to the effect of ring dust materials. However, the ENA imaging capabilities of INCA, combined with the information of energy spectra, angular distribution, and charge state obtained with LEMMS and CHEMS, provides a powerful new technique for diagnosing ring-particulate/ energetic-particle interactions, as described below.

The intense populations of magnetically trapped, energetic charged particles that constitute the radiation belts of Saturn's inner magnetosphere are slowly transported towards the planet by radial diffusion processes. Many of them interact with the rings of Saturn and ultimately are lost to the magnetospheric system. Energetic protons with energies greater than ~50 keV will completely penetrate ring particulates with diameters in the sub-micron regime, such as those that are key constituents of the F, G, and E rings of Saturn. A substantial fraction of those penetrating protons (~60% at 50 keV) will emerge neutralized by the interaction, ending up as hydrogen ENAs. Thus, the interactions between the trapped energetic particles and the ring particulates may be observed remotely by an ENA camera that measures the energy, mass species, and the arrival direction of ENAs. The ability of the INCA

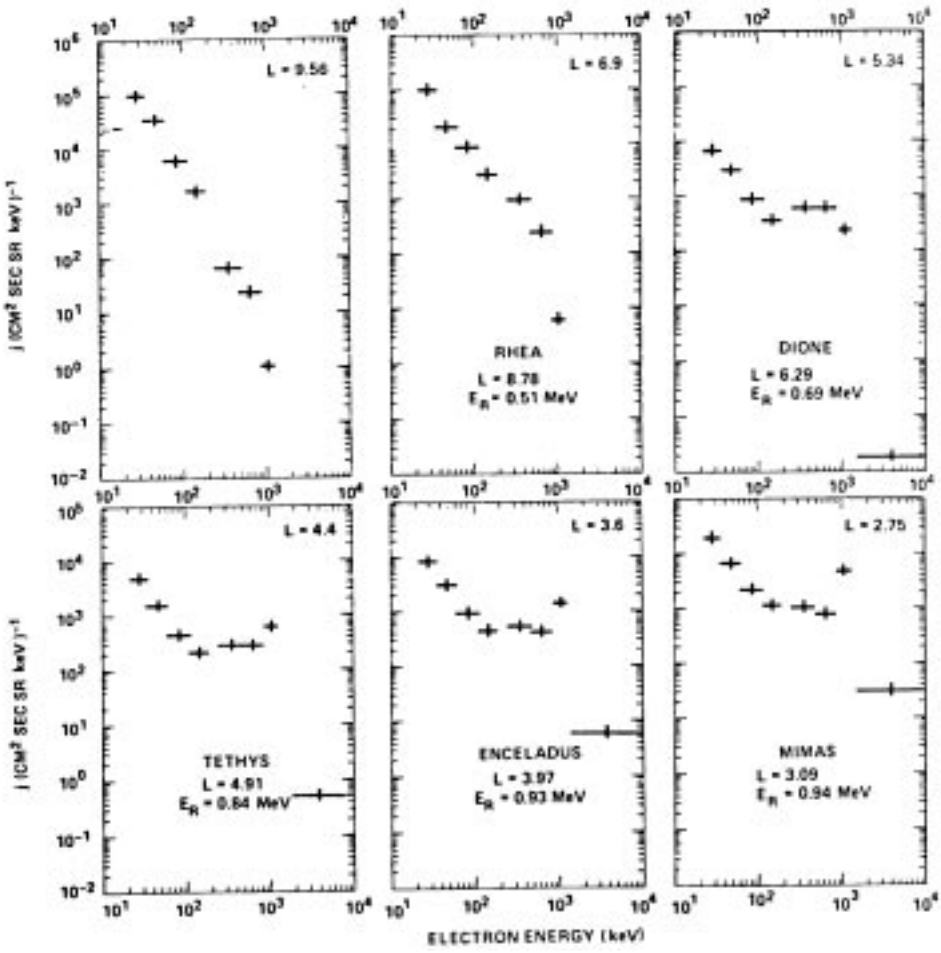

Figure 2.3. The evolution of the electron energy spectrum at various L values, upper left to lower right, as registered by LECP on Voyager 2. The L values are indicated in each panel, and the resonant electron energy E_R at each satellite is shown in successive panels. From Krimigis et al. (1982a).

sensor of the MIMI instrument to image energetic-particle/ring-particulate interactions within Saturn's inner magnetosphere during the Saturn Orbit Insertion (SOI) phase of the Cassini mission was recently documented by Mauk et al. (1998). A simulated ENA image of Saturn's F-ring from that work is shown in Figure 2.5. Mauk et al. (1998) showed that with such images we can obtain powerful new diagnostics of magnetospheric radial transport of energetic charged particles. Also, the impact rates for the consideration of sputtering and erosion will be better constrained, and the relative importance of the rings as a sink of radiation belt particles will be

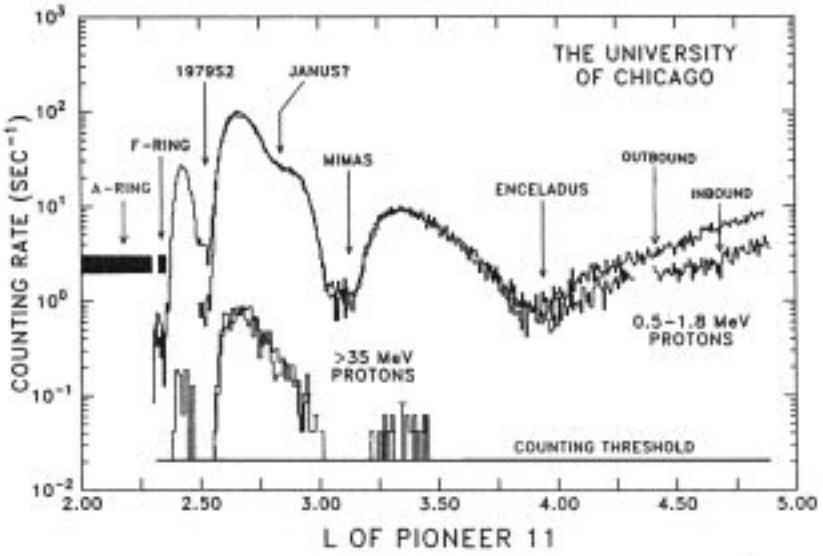

Figure 2.4. Energetic ions measured by Pioneer 11 in Saturn's inner magnetosphere. (After Simpson et al., 1980).

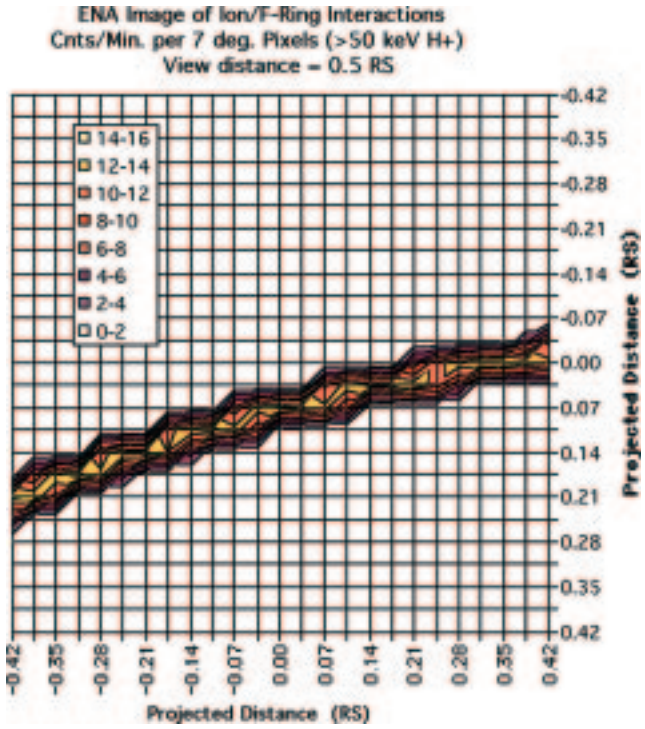

Figure 2.5. Simulated ENA image of a portion of the F-ring as it might appear to the INCA MIMI ENA camera on the Cassini spacecraft at a distance from the ring segment near the center of the image of 0.5 R_S during the Saturn Orbit Insertion phase of the mission. The units are counts per minute. The F-ring dust particulates are assumed to have a size of 0.5 mm. A lower limit assumption has been made concerning the radial transport of energetic protons (~ 0.01 km/s). After Mauk et al. (1998).

determined. Finally, the energy spectra of the ENA emissions will provide a new type of constraint on the size distribution of the ring particulates. Figure 2.6 shows a sample of the modeled sensitivity of the ENA spectra to the dust particulate sizes.

2.3 Saturn Charged Particle Environment

Saturn's magnetosphere is a prodigious accelerator of charged particles, as apparently are the magnetospheres of all strongly magnetized planets. There is no clear understanding why planetary magnetospheres have this characteristic. Saturn's magnetosphere has unique properties that can help unravel the relative importance of various proposed mechanisms for particle acceleration and transport. Saturn's energetic particle population is also unique in the degree of interaction between the

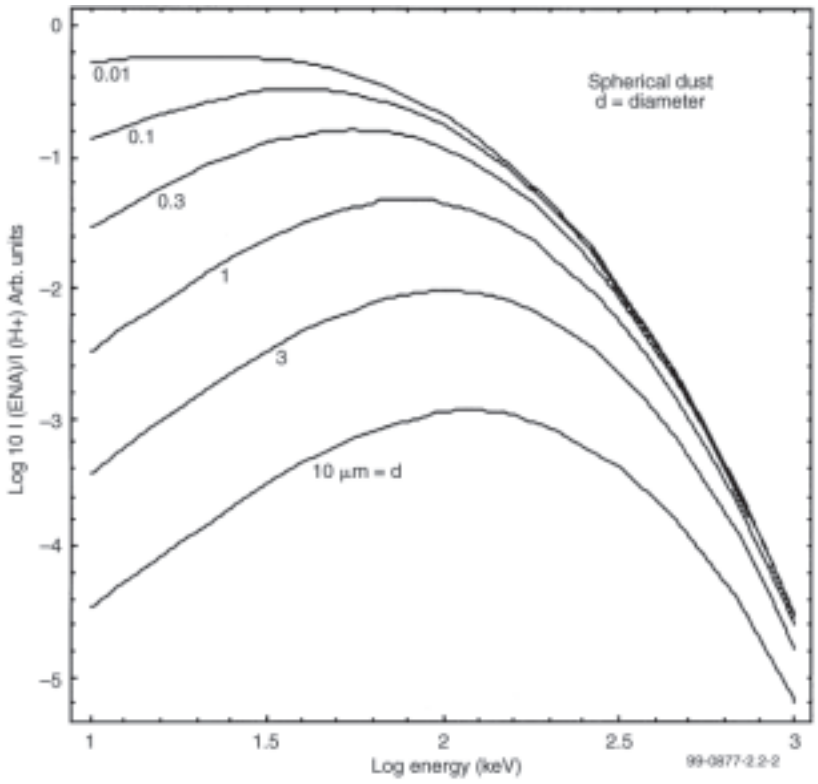

Figure 2.6. Model calculations of ENA emission energy-spectra from the dust particulates as a function of particulate size and shape. The spectra are normalized by the parent ion spectra. It was assumed the dust particulates are spherical. Other simulations given by Mauk et al. (1998) test for sensitivity to particulate shape.

charged particle populations and the neutral and solid materials such as planetary gases, dust and ring materials, and satellite surfaces. Thus, Saturn's magnetosphere may come closest to emulating the conditions that existed within the Sun's planetary nebula and during later stages in the formation of the solar system.

Figure 2.7 shows Saturn's energetic charged particle environment as characterized with the Low Energy Charged Particle (LECP) instrument on Voyager 2 (Krimigis et al., 1983). Energetic particles fill the magnetosphere to the dayside magnetopause and participate in the force balance of the magnetosphere with the interplanetary environment. Energetic particles clearly leak out of the magnetospheric boundary. Strong inbound/outbound (dayside/predusk) asymmetries have been interpreted as being the result of temporal dynamics. Shorter-scale temporal dynamics are also apparent in the so-called "mantle" region (inbound-dayside, $r > 10\ R_S$), undoubtedly related to dense, detached, cold plasma regions, apparently shed from

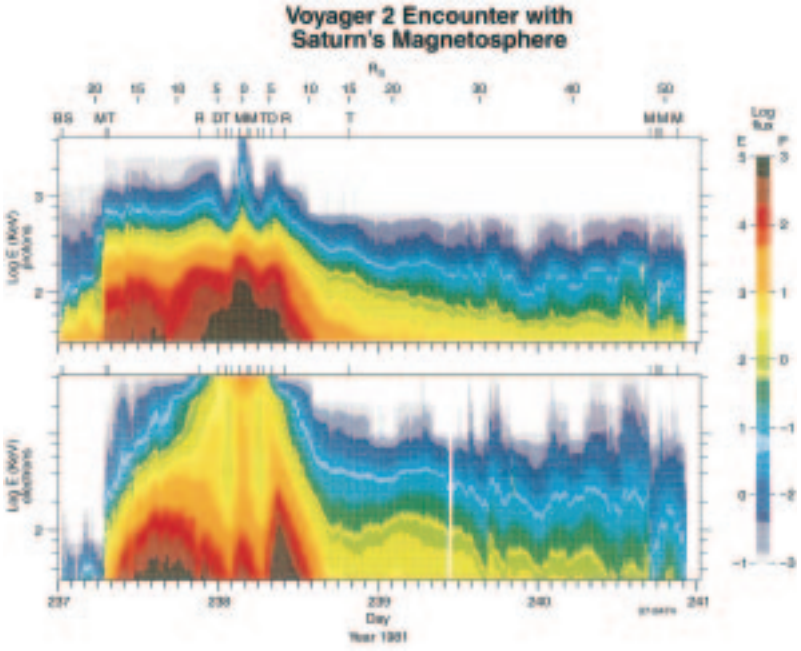

Figure 2.7. Color spectrogram of energetic ions (top) and electrons (bottom) measured by Low Energy Charged Particle (LECP) instrument on Voyager 2 during its encounter with Saturn. The color is coded according to the $\log_{10}$ of intensity [(cm s sr keV)$^{-1}$]. Radial distance (in R_S) is given below each color panel, and various events are given above each panel. The events are: BS = bowshock, M (first and last 3) = magnetopause, T (first and last) = Titan *L*-shell, R = Rhea *L*-shell, D = Dione *L*-shell, T (middle 2) = Tethys *L*-shell, and M (middle 2) = Mimas *L*-shell. The unlabeled tick marks between Tethys and Mimas represent the Enceladus *L*-shell. After Krimigis et al. (1983).

the interior plasma sheet (Sittler et al., 1983). Large-scale modulations observed in the outbound regions, apparently related to the Saturn rotational modulations reported from the Voyager 1 encounter (Carbary and Krimigis, 1982), are surprising, given the near-exact alignment of Saturn's magnetic axis with its spin axis. Energetic particles in the inner regions show the clear signatures of strong interactions with materials, including the natural satellite surfaces. The very peculiar electron spectra near closest approach (Krimigis et al., 1982a), showing the intensities rising at the highest energies, are interpreted as being the signature of a drift period resonance with orbital period of the satellites (see Figure 2.3).

The temporal dynamics mentioned above are of particular interest for the MIMI investigation of the Saturnian system. Saturn's magnetosphere is thought to occupy a middle ground between magnetospheres such as that of Earth, whose dynamics and energetics are determined by a strong interaction with the interplanetary medium, and magnetospheres such as that of Jupiter, thought to be controlled predominantly by the rapid rotations of the central planet. By comparing the energetic particle characteristics, and their temporal dynamics among Earth, Jupiter, and Saturn, we will be able to sort out the relative influences of rotational and interplanetary environment on the energization of charged particles to high energy. Temporal dynamic processes at Earth are well characterized, and Galileo is now shedding substantial light on the energetic particle dynamics at Jupiter. MIMI will provide for an unprecedented characterization of the energetic particle dynamics within the Saturnian magnetosphere.

The critical influence of such materials as dust, rings, and satellite surfaces on the character of the energetic particle populations is shown most clearly in Figure 2.4 (Simpson et al., 1980). Dust particulates of the F, G, and E-rings clearly have roles to play, as do both the larger particles of the A and F rings and the satellites. Ring interaction signatures are highlighted further in Figure 2.8 with the 90° bite-outs observed in energetic particle pitch angle distributions measured near the G-ring (Krimigis and Armstrong, 1982). Also, the very high energy component of the spectra shown (the bump at ~100 MeV) has been interpreted as resulting from CRAND from impacts on the rings. LEMMS will be able to measure these features at all local times, various distances, and latitudes over the entire mission of at least 4 years.

Energetic particle composition is another clear signature of the importance of materials interactions for establishing the character of the energetic particle populations. Figure 2.9 shows that both Jupiter's atmosphere (H_2, H_3) and the solar wind

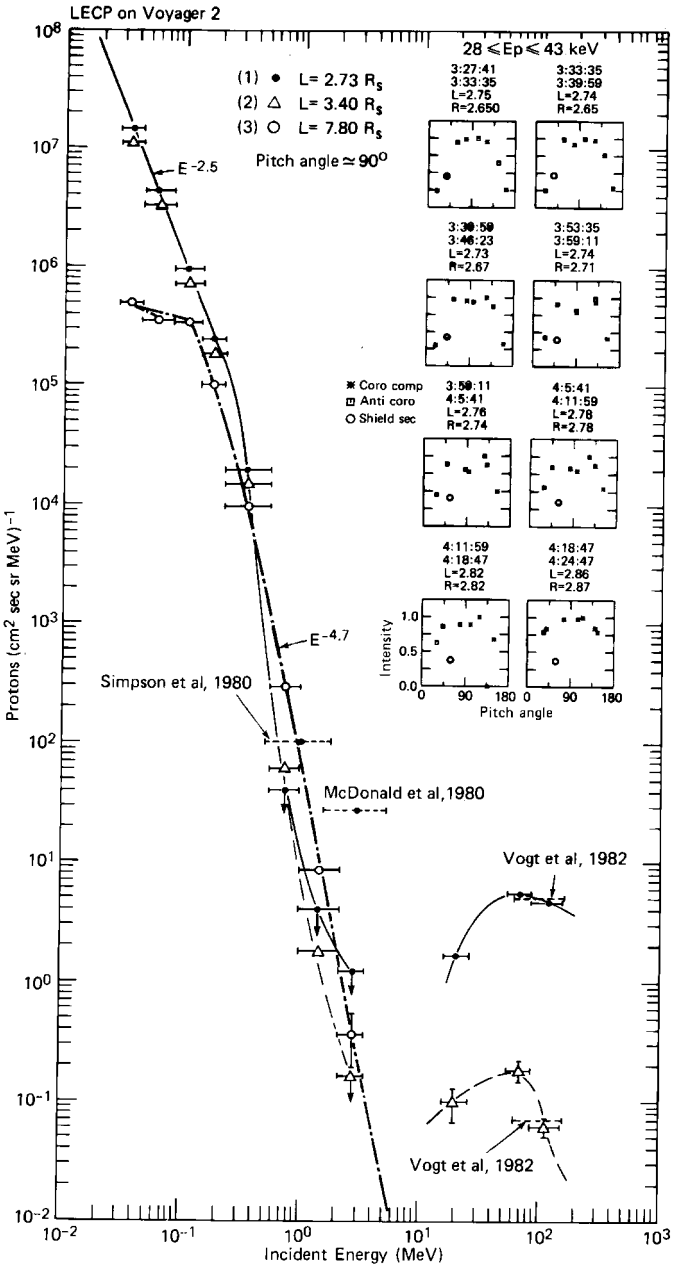

Figure 2.8. Spectra and pitch angle distributions of energetic ions measured in Saturn's inner magnetosphere by Voyager 2 and comparison with Pioneer-11. After Krimigis and Armstrong (1982).

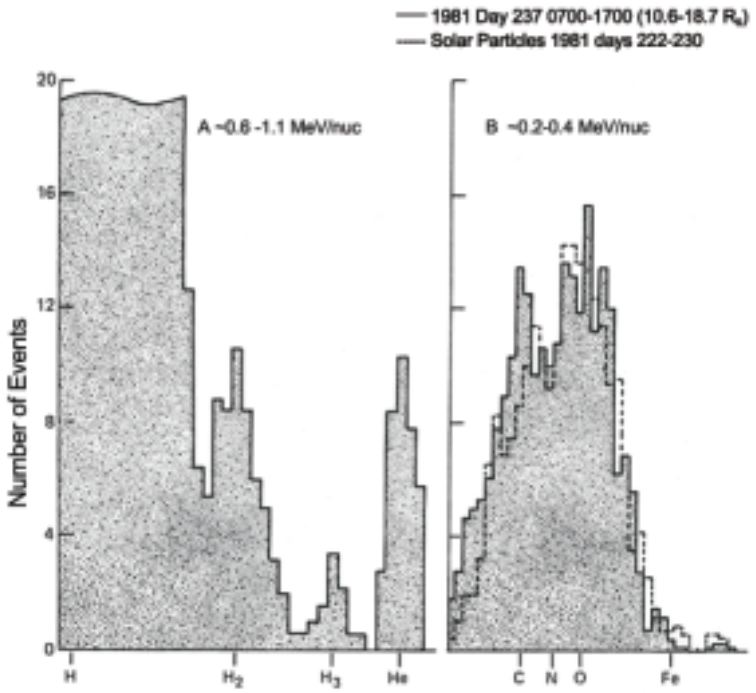

Figure 2.9. Composition distribution of energetic ions measured by Voyager 2 in Saturn's middle magnetosphere. After Krimigis et al. (1982b).

(He) are contributors to the energetic particle populations, and the presence of heavier ions (C, N, O) are possible tracers of satellite and ring sources (Krimigis et al., 1982b). Evidence not shown here (Krimigis et al., 1983) suggests that oxygen ions dominate the energy density of the ion populations planetward of ~6 R_S, indicating that sputtering off the icy satellites may be a dominant source of energetic particles in these regions. The relative strengths of all sources, particularly of Titan versus the icy satellites, is not known. MIMI, with compositional and charge state discrimination capabilities that dwarf previous measurements at Saturn, will establish where the energetic particles come from.

Dust, ring particles, satellites surfaces, and gas distributions help determine the characteristics of the energetic particles, but these materials are in turn modified by the energetic particles. Energetic particles process and change the surfaces of materials (e.g., Johnson, 1990), and they affect the transport of dust, and perhaps larger ring particles (Goertz, 1989; Mendis et al., 1984). The use of MIMI in concert with the comprehensive suite of Cassini instruments (e.g. UVIS measurements of gas

distributions, Imaging Science Subsystems (ISS) images of dust distributions, etc.) will allow for an epochal characterization of the solar nebula-like interactions that are now occurring within the Saturnian system.

MIMI will also provide unprecedented new information about several other aspects of the Saturnian energetic particle populations that have remained ambiguous since the Voyager encounters. Previous limitations in ion compositional analysis and angular resolution and coverage have prevented us from achieving closure in the analysis of force balance between magnetic fields and plasmas (Mauk et al., 1985). Saturn appears to be unique in the interplay that exists between the contributions of cold and hot plasmas in balancing magnetic stresses. Pressure gradient and anisotropy effects appear to dominate ring current generation in the inner and middle regions, as at Earth, whereas corotational stresses dominate in the outer regions, as was once thought to be true at Jupiter. We will now have the opportunity of obtaining information about stress balance at Saturn that will tell us a great deal about how such balance is achieved in planetary magnetospheres in general. These same measurement limitations (composition, angular information) have also resulted in very wide uncertainties in our knowledge of radial transport rates of energetic particles at Saturn (Paonessa and Cheng, 1986). Phase space density analyses of the energetic particle populations, in the context of radial diffusion theory (Schulz and Lanzerotti, 1974), should constrain the radial transport and loss rates to a much higher precision than previously available once accurate charged particle invariant parameters are established (with improved angular coverage and resolution) and once the compositional state of the energetic particles can also be established.

2.4 Titan Interactions

Titan's nitrogen-rich atmosphere is subject to direct magnetospheric interaction due to its lack of a significant intrinsic magnetic field. To some extent, the dynamical process will be similar to the solar wind interaction with Mars or comets, with the major difference that no bow shock will form because the local value of the magnetosonic Mach number is less than one. The Voyager 1 plasma measurements at Titan flyby showed that a well-defined magnetotail was formed in the wake

region (Ness et al., 1982). However, a four-lobe configuration can also be deduced from both the magnetometer and plasma wave observations (Ness et al., 1982; Gurnett et al., 1982; Neubauer, 1992). This unique phenomenon is caused by the finite gyroradius effect of the exospheric ions created in the vicinity of Titan. This also suggests that Titan's exospheric and ionospheric structures should be highly asymmetric because of the preferential sputtering of the pickup ions on the hemisphere opposite to Saturn. The immediate consequence for the MIMI instrument is that such exospheric structures could be revealed by the ENA images in detail (see Amsif et al., 1997). (We expect a more extensive structure of Titan's exosphere on the anti-Saturn side because of the reimpact effect of the pickup ions.) The MIMI experiment can also be used to study the possible occurrence of particle acceleration in the magnetotail of Titan.

On a global scale, the injection of nitrogen and carbon ions from Titan's exosphere into the Saturnian magnetosphere also provides an ideal set of tracer particles to follow the transport process of energetic ions. The possible detection of molecular ions such as CH^+_3, CH^+_5, and H_2CN^+ created in Titan's ionosphere (Ip, 1990) could also be used to diagnose time-dependent mechanisms since their lifetimes are limited by electron dissociative recombination.

As indicated, the very weak or nonexistent intrinsic magnetic field of Titan gives the Kronian magnetospheric plasma direct access to the upper Titan atmosphere, where a variety of complex phenomena take place (Eviatar, 1992; Ip, 1992). Energetic ions in the magnetosphere occasionally will undergo a charge exchange collision with cold neutral atoms from the upper Titan atmosphere, giving rise to the production of ENAs. The energy of the incident ions is almost entirely transferred to the charge exchange-produced ENAs, which then propagate along nearly rectilinear ballistic trajectories. The coexistence of energetic ions and cold tenuous gas in the Saturn/Titan system thus makes this system particularly suitable for magnetospheric imaging via ENAs (Cheng and Krimigis, 1989b; Curtis and Hsieh, 1989).

The first simulated ENA images of the Saturn/Titan system are due to Hsieh and Curtis (1988), who modelled the Titan torus around Saturn. Later, Roelof and Williams (1990) included Titan itself, and further examples were presented by Cheng

et al. (1993). ENAs emitted from the Saturn magnetosphere were detected (without imaging) by the LECP instrument onboard Voyager 1, which was designed to detect mainly charged particles, so there was no system to reject the ions (Kirsch et al., 1981a; Cheng, 1986). The observations were made during periods when Voyager 1 was on open field lines, where there were no significant ion fluxes. The emission was modeled by Hsieh and Curtis (1988).

Amsif et al. (1997) presented a study of the energetic neutral atom production, resulting from the interaction of Titan's exosphere with Saturn's magnetosphere. This necessitated the development of a model for the altitude density profile and composition of both the inner and the outer exosphere of Titan. They used a Chamberlain model for the inner exosphere (altitude < 6000 km), for particles with ballistic and escaping orbits, and included the five major species: H, H_2, N, N_2, and CH_4. The exospheric density and composition altitude profiles obtained from this model were then used in order to calculate the fluxes and the energy spectra of the ENAs produced in the "inner exosphere" of Titan, considering a proton spectrum measured by Voyager in the Saturnian magnetosphere as the parent ion population (Krimigis et al., 1983). The results show how the exospheric species contribute in a different way, as a function of altitude, to the ENA flux spectra. For look directions that go from the Cassini orbiter almost all the way down to the exobase, the contribution to ENA production comes mostly from charge exchanges with CH_4 and N_2. This not only is due to the high integral column density of these molecules, but also is mainly the result of their high charge exchange cross sections. H_2 has also high integral column densities, but its lower charge exchange cross sections significantly reduce its contribution to the ENA fluxes. This sensitivity of ENA production to the composition of the neutral atmosphere means that the ENA directional fluxes and spectra, which MIMI will measure, will constitute a powerful diagnostic tool for evaluating the abundance of the different species in the layers of the Titan exosphere. The calculated spectra of the ENAs are also much softer than the spectrum of the parent energetic ion population. This is due to the filter effect of the charge exchange cross sections, which decreases the efficiency of ENA production at high energies.

In the outer exosphere (altitude > 6000 km), molecular hydrogen is the dominant species, and a Chamberlain model that included H_2 particles with ballistic, satellite, and escaping orbits was utilized to evaluate the altitude density profile. This permits an estimate of the ENA intensities several Titan radii from the moon and was used to simulate a flyby of Titan, from 1 day before closest approach to 1 day after, just as will occur about 40 times during the Cassini orbiter tour. Figure 2.10 (Amsif et al., 1997), shows such a simulated flyby for the 24 hours following Titan closest approach. Times are given in hours (H) or minutes (M). The images in each panel are Mercator projections of the entire sky as viewed from the Cassini spacecraft. ENA intensity is shown in the left panels, and equivalent neutral hydrogen column density in the right panels. Near Titan, the molecular H_2 densities were treated as atomic H densities of twice the value. The coordinate system is Sun-Saturn-ecliptic, with the azimuth angle plotted horizontally (in values decreasing from approximately 360° on the left of the panel to 0° on the right, both 0° and 360° being the sunward viewing direction), and the elevation angle plotted vertically (increasing upwards from –90° to +90° relative to Saturn). Coordinate labels are suppressed because of the small size of each panel. A logarithmic color bar has been used, covering a range from the maximum value to 1/100 of that value, for both the ENA unidirectional intensity j_{ENA} (left panels) and column density h (right panels). The maximum values for each panel are given in dimensionless units scaled for convenience so that the maxima from the numerical computation would be of order unity. The Titan exosphere is nearly as bright in ENA as the inner magnetosphere of Saturn, making it possible to image the exosphere out to at least 5 Titan radii, and even to resolve it when the spacecraft is several Saturn radii distant from the moon.

In Figure 2.10 it is assumed that the energetic ion population in the vicinity of Titan is uniform and that its pitch angle distribution is isotropic. Well away from the moon these simplifications are the most justifiable. Near Titan, however, and possibly in the vicinity of its wake, finite Larmor radius effects will be important. As an example, a 20 keV proton in a 5 nT magnetic field, as was measured by Voyager near Titan (Neubauer, 1992), has a ~4000 km gyroradius. This is comparable to the Titan exobase radius, which is about 4175 km. Some dark areas in the ENA

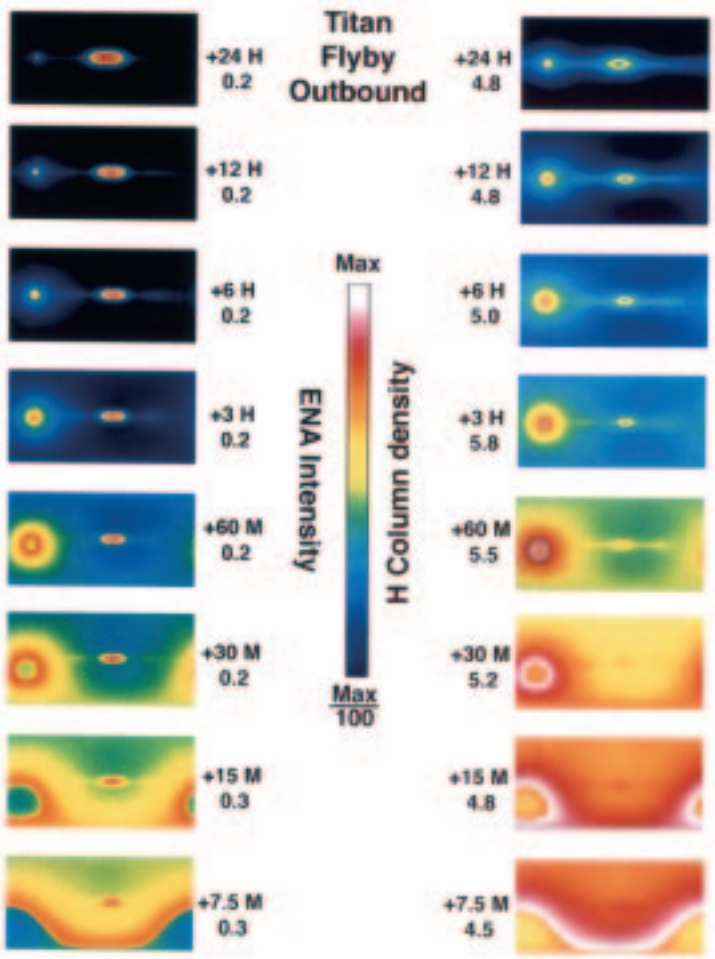

Figure 2.10. ENA intensity (left panels) and equivalent neutral hydrogen column density (right panels) for a simulated outbound Titan flyby of Cassini Orbiter. Where hydrogen is molecular (Titan exosphere), density is 2 [H_2]. Mercator projections of the entire sky (–90° to +90° in elevation centered on Saturn, and 360° in Saturn equatorial azimuth, centered for each panel so as to include both Saturn and Titan). Bold numbers are times relative to closest approach (M = minutes, H = hours). Logarithmic color bar (factor of 100) normalized to brightest pixel in each panel. Maximum values in each panel given as dimensionless numbers. Multiply dimensionless column densities by 1.2×10^{13} cm^{-2} (cf. Amsif et al., 1997). Distant Saturn magnetosphere (brightest points are ring current at $L \cong 3$) is comparable in ENA brightness to Titan exosphere, while Titan hydrogen torus (idealized) is much weaker. Note ENA image of Titan exosphere is distinct from Saturn magnetosphere (except within an hour of closest approach).

images are thus expected, in the one side of Titan, due to the screening effect from Titan and its lower atmosphere. In order to simulate these effects, a 3-D model of the interaction of Titan's exosphere with Saturn's magnetosphere has been developed (Amsif, 1996; Dandouras and Amsif, 1999). This necessitated 3-D trajectory tracing techniques for each ion. The results are shown in Figure 2.11, where a Titan

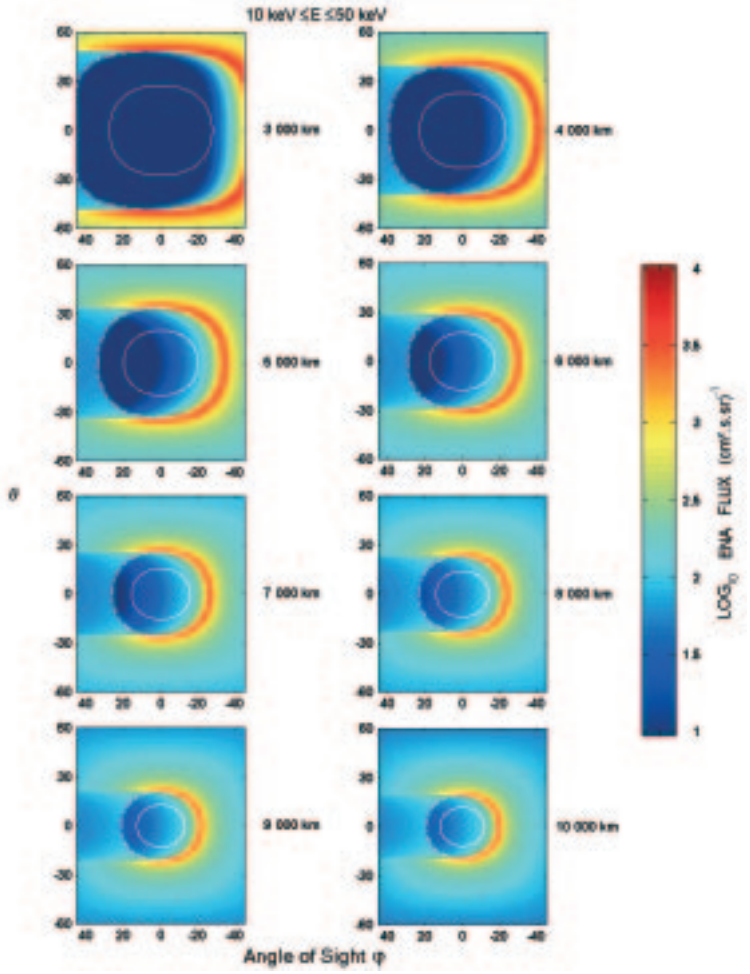

Figure 2.11. ENA flux as a function of the azimuth view angle ϕ and the elevation view angle θ, for eight altitude values of the Cassini orbiter above the Titan surface, ranging from 3000 to 10 000 km. The ENA energy range is 10–50 keV, and the images correspond to the INCA field of view (90° × 120°). The continuous white circle represents the Titan surface, and the dashed white circle represents the Titan exobase. (Dandouras and Amsif, 1999).

flyby image sequence is simulated, for selected altitude values. Limb brightening effects above the Titan exobase are very clear in these images, and are due to the integrated optical depth in an optically tenuous medium, at certain grazing angles. The other salient feature is shadow effects in the ENA images of the Titan exosphere, which as explained above are due to the finite gyroradii of the parent ion population and the screening effect of Titan. These shadows depend on the ENA energy, on the relative geometry of Titan, and on the magnetic field and the location of the Cassini spacecraft. The INCA images will thus allow remote sensing, not

only of the ion fluxes and spectra, but also of the magnetic field in the Titan vicinity. The magnetospheric imaging technique via energetic neutral atom detection is thus a powerful diagnostic tool for the interaction of Saturn's magnetosphere with Titan.

Typical ENA fluxes over Titan are generally of the order of 200 to 3000 $cm^{-2} \cdot s^{-1} \cdot sr^{-1}$. By taking into account the geometrical factor of the INCA ENA imager, which is ~2.4 $cm^2 \cdot sr$ for the full 90° × 120° field of view, and considering 32 × 32 pixel images with 86-s exposure (high time resolution images), we get on the order of 40 to 600 counts/pixel in the 10–50 keV energy range. This corresponds to Poisson uncertainties in the 4–15% range (at 1 σ), showing the capabilities for performing magnetospheric imaging studies of the Titan–Saturn interaction with good resolution.

Note that the spacecraft velocity effects on this type of imaging are minimal. For a typical Titan flyby, the Cassini relative velocity is ~5.9 km/s, which corresponds to a ~507 km interval along the spacecraft trajectory during the 86 s exposure. If we take as an example a 2781-km minimum altitude flyby, the spacecraft altitude evolves from 5000 to ~4640 km, which corresponds to an evolution of the angle φ, for the exobase, from 33.5° to 35.4°. The resulting $\Delta\varphi = 1.9°$ is smaller than the 2.8° pixel resolution of the ENA images in the high time resolution images (90° × 120° field of view).

2.5 Auxiliary Science: Jupiter and Interplanetary Particle Environment

2.5.1 *MIMI Measurements at Jupiter*

In December 2000, the Cassini spacecraft obtained a gravity assist from Jupiter as it heads toward Saturn. It encountered the Jovian system with a closest approach distance of ~139 R_J at ~1600 local time (LT). Several aspects of the Cassini encounter with Jupiter have made it possible to address key science questions about Jupiter's space environment that other missions, including Galileo, have not been able to address as effectively or at all. Among these aspects are the unique capabilities of the MIMI instrument. In particular, at Jupiter the MIMI instrument has (Krimigis et al, 2002):

(1) Provided the first global magnetospheric images of Jupiter using the ENA imaging capabilities of INCA head. The ability of MIMI to obtain high-quality images of Jupiter's inner and middle magnetosphere ($r < 30\ R_J$) during Cassini's gravity-assist flyby was documented by Mauk et al. (1998). A simulated raw image of Jupiter as it would be viewed by INCA from a distance of ~139 R_J is shown in Figure 2.12. The color is coded according to $\log_{10}$ of the counts received in 3 hours. Approximately 160 of these images have been obtained over a 20-day period, even while Cassini's main communications antenna remained pointed toward the Earth. The images will be sorted and summed according to the variations in systems drivers, including solar wind variations, Jupiter's rotation, the orbital position of Io, etc. The circle shows the anticipated resolution of the INCA measurements after deconvolution procedures have been applied. We expect to separately characterize the regions planetward of ~10 R_J, the transition region between dipolar and magnetodisc configurations (10–20 R_J), and the magnetodisc regions out to beyond ~30 R_J. This analysis is currently in progress.

(2) Provided the first measurement of the relative concentrations of singly to multiply charged energetic heavy ions using the Cassini MIMI/CHEMS head. The Ulysses SWICS instrument made the first measurements of energetic ion charge states in Jupiter's magnetosphere (Geiss et al., 1992), but was unable to uniquely

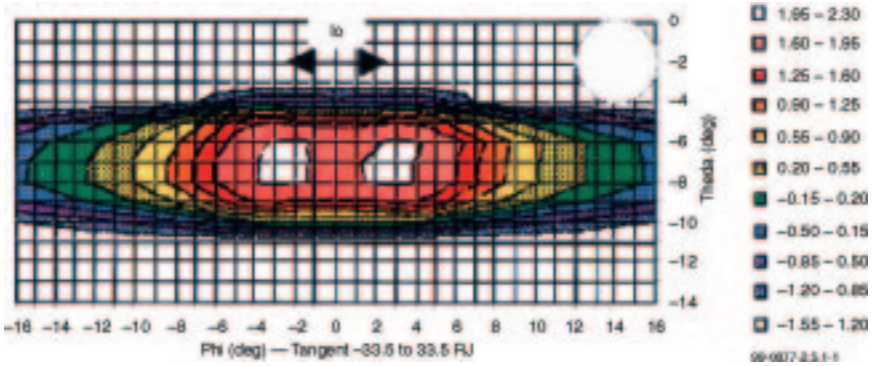

Figure 2.12. Simulation of an ENA (hydrogen) image of Jupiter's magnetosphere as it would appear to the MIMI/INCA head from 139 R_J and 5° magnetic latitude. Color is coded according to the $\log_{10}$ of counts of 60–120 keV H atoms as observed within 4° angular pixels for a 3-hour accumulation. Deconvolution would result in a much thinner (more pancake) structure. The circle shows angular resolution capabilities of INCA after deconvolution.

identify singly charged oxygen and was essentially blind to singly charged sulfur (Geiss et al., 1992). MIMI/CHEMS is the first instrument at Jupiter capable of making this discrimination. More sensitive than the SWICS instrument by a factor of ~30, CHEMS has been able to sense the charge state distributions of the outer magnetospheric regions remotely by characterizing the charge state distributions of pickup ions (PUIs) and other upstream ion events. These events are common in the upstream solar wind regions near Jupiter and are heavily laden with heavy ions from Jupiter's outer magnetospheric regions and the Io torus (Zwickl et al., 1981; Krimigis et al, 1985; Barbosa and Eviatar, 1986).

With these capabilities the Cassini MIMI instrument will play a critical role in addressing several outstanding questions regarding the Jovian system including:

(a) *What is the influence of the interplanetary environment, relative to other drivers, on the structure and dynamics of Jupiter's magnetosphere and what are the mechanisms by which such influence is exercised?*

The dynamics of Jupiter's magnetosphere are driven predominantly by planetary rotation (Gehrels, 1976; Dessler, 1983). However, the Jovian magnetosphere is much more dynamic than might be anticipated in a system controlled largely by "rock-steady" planetary rotation, and there is increasing evidence that the interaction with the interplanetary medium can exercise an important influence on magnetospheric processes (Desch and Barrow, 1984; Reiner et al., 1993; Kaiser, 1993; Baron et al., 1996; Clarke et al., 1996; Satoh et al., 1996; Prangé et al., 1993; Schneider and Trauger, 1995; Mauk et al., 1999). The MIMI/INCA head has obtained ENA images that could illuminate the dynamics of Jupiter's inner and middle magnetosphere while other instruments (Dual Technique Magnetometer (MAG), Cassini Plasma Spectrometer (CAPS)) are monitoring the conditions of the interplanetary environment. These images may discriminate structures that are influenced by interplanetary conditions from those that are not.

(b) *How are hot plasmas transported and energized to generate and support Jupiter's unique magnetodisc configuration?*

It is now known that the magnetodisc is predominantly supported by pressures and pressure anisotropies in the sparse, hot plasma components (Mauk and Krimigis, 1987; Paranicas et al., 1991). We do not know how these hot plasmas are energized and transported, and therefore we cannot begin to understand how these populations are able to form the magnetodisc configuration. According to the "neutral wind" model, corotating Io torus ions are neutralized by charge exchange, re-ionized in the middle and outer magnetosphere by photoionization, energized by pickup and other processes, and then transported back towards the planet by global radial diffusion processes (Eviatar et al., 1976; Barbosa et al., 1984). Alternatively, Io torus plasmas may be transported outward as a cold component by plasma processes, energized, and then transported inward as a hot component. The charge state of the hot heavy ions provided by the MIMI/CHEMS head, and the angular distribution together with the energy spectral shape provided by MIMI/LEMMS, yield a unique fingerprint of the neutral wind model, because according to this model, singly charged ions would be very strongly favored when compared with the charge states measured in the Io torus (Belcher, 1983). Once the transport mechanism is established, researchers can then address mechanisms of magnetodisc formation.

Additionally, the Cassini spacecraft has been the first spacecraft to visit the dusk flanks of the Jovian magnetosphere near the equatorial plane, complementing Ulysses' high-latitude pass. This unique opportunity allows for the completion of the "exploration" of Jupiter's broad magnetospheric region. Of particular interest are the indications of solar wind and boundary layer flow, and the associated draping of the magnetic field configuration inside the dusk flank magnetosphere, as a signature of the strength of interactions between the solar wind flow environment and the corotating magnetospheric plasmas (Cheng and Krimigis, 1989a). Observations of detached Jovian plasmas may provide signatures of the plasma shedding processes in the outer Jovian magnetosphere.

2.5.2 *Pickup Ions*

Before arriving at Saturn, the Cassini spacecraft will spend half a solar cycle in interplanetary space, providing a unique opportunity to study in detail a variety of interplanetary particle populations and acceleration processes. MIMI/CHEMS with its large geometry factor and its ability to measure charge states and resolve ion species (e.g., N from O), will provide detailed information on the variations of these populations with radial distance and solar activity. Of particular interest will be (a) interstellar pickup ions (and the low energy portions of the anomalous component); (b) ion acceleration, especially at high-Mach number shocks and in Corotating Interaction Regions (CIRs); and (c) bowshock processes upstream of Saturn and Jupiter (including leakage of energetic ions from the magnetospheres of these planets).

The presence of pickup ions in the inner solar system (~1 to 5 AU) is now well established (e.g., Gloeckler et al., 1993; Geiss et al., 1994; 1995; Gloeckler, 1996; Mall et al., 1998; Gloeckler and Geiss, 1998). Investigation of the characteristics of this important heliospheric ion population has already revealed fundamental information about the acceleration of these suprathermal ions (Gloeckler et al., 1994; Fisk et al., 1997), as well as properties of our local interstellar cloud (Gloeckler and Geiss, 1996; Gloeckler et al., 1997; Gloeckler and Geiss, 1998) that could not otherwise be obtained.

The Cassini orbit and the excellent capabilities of CHEMS will make it feasible to gain new information on pickup ions and to measure pickup Ar for the first time. With continuing pickup ion measurements at 1 AU on ACE and from ~1.5 to ~5.5 AU on Ulysses, together with the recent results from Voyager-1 (Krimigis et al, 2000), the Cassini MIMI observations are essential for providing us with a good global, 3-D view of the spatial distribution of neutrals in the heliosphere. Examples of some of the anticipated results are described below.

2.5.2.1 Composition of the Interstellar Cloud

Because the density of pickup ions (except for He) increases almost exponentially with increasing distance from the Sun, Cassini MIMI measurements at ~10 AU with a more sensitive instrument (CHEMS) than those on Ulysses and ACE will give us

the most precise information on the composition of pickup ions. In Figure 2.13 the pickup O^+ spectrum obtained with Ulysses at ~5 AU is shown. The data used were averaged over a 5-month period in order to reveal the spectral shape in sufficient detail to identify both the interstellar and inner source for oxygen. With CHEMS at 10 AU the statistical accuracy of pickup ion measurements will improve by about a factor of 10. This will lead directly to establishing accurate elemental (and in some cases isotopic) abundances in the local interstellar cloud surrounding our solar system, information of considerable importance for models of stellar evolution. It will also provide powerful constraints on acceleration models for anomalous cosmic rays.

2.5.2.2 Ionization Rates of the Neutral Gas

Analysis of the distribution functions of pickup ions measured by CHEMS over a range of heliocentric distances (~3 to 10 AU) combined with similar measurements by SWICS on Ulysses, will give us our best determination of ionization loss rates of the various interstellar neutral species (e.g. H, N, O, Ne) inside the heliosphere.

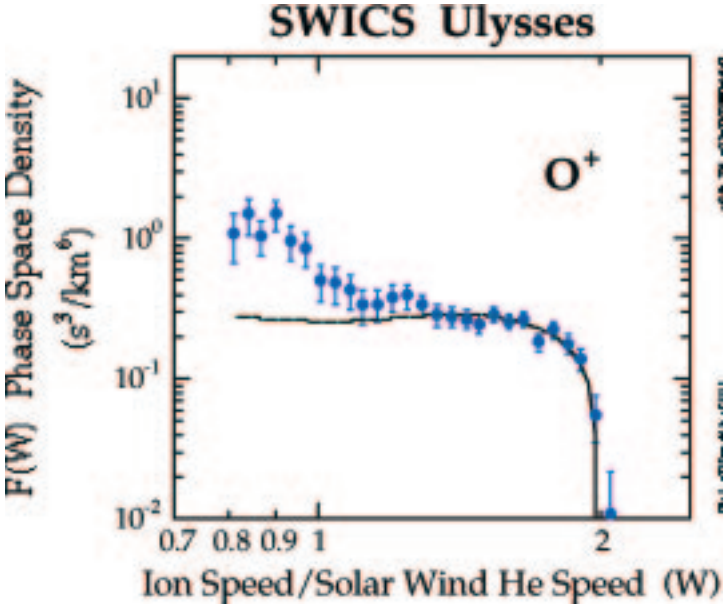

Figure 2.13. Ulysses SWICS observations of the phase-space density of O^+ averaged over 135 days from from 17 February to 1 July 1992. The average solar wind speed was relatively steady at 442 ± 36 km/s and the distance from the Sun remained close to 5.4 AU during the entire time period of these observations. The curve is the model calculation of interstellar pickup O^+. While the agreement between the model and data is excellent above W of about 1.3, a significant amount of O^+ from another source is evident below $W \sim 1.2$. Adapted from Figure 10 of Gloeckler and Geiss (1998).

Knowledge of these ionization rates is essential for deriving accurate interstellar abundances.

2.5.2.3 Temperature of the Interstellar Gas

Measurements of the spatial variations of pickup ions with Cassini MIMI as its orbit crosses the so-called gravitational focusing cone (e.g., Holzer, 1977) gives us the only chance to determine the temperature of several atomic species (e.g., O, N, Ne) in the local interstellar cloud. Combining this with knowledge of the atomic He temperature (Witte et al., 1996) will give clues to how this warm cloud is heated.

2.5.3 *Upstream Particle Events: Bowshock Processes and Magnetospheric Leakage*

Cassini will spend most of its first 15 orbits upstream of the Saturnian bow shock. MIMI/INCA with its large geometry factor in the ion mode is ideal for studies of upstream ion activity, originally observed by Voyager 1 and 2 (Krimigis et al., 1983; Krimigis, 1986) out to ~200 R_S. The early Cassini apoapses lie in the dawn sector, where the spiral interplanetary magnetic field is most likely to connect to the bow shock. Substantial upstream particle activity is therefore expected and will be detected by MIMI/LEMMS. During the Voyager 2 flyby, upstream ion bursts were present at least half the time (Krimigis et al., 1985).

At a planetary bow shock, solar wind ions are reflected into the upstream region. Theories of first-order Fermi acceleration (e.g., Lee, 1982) suggest that such ions should act as a seed population for diffusive acceleration by ion-generated irregularities upstream of the bow shock. Cassini measurements offer the opportunity to perform extensive tests of this model at a planetary bow shock with higher Mach number and much larger dimensions than at Earth. The acceleration region upstream of Saturn is at least ten times larger, so that the cutoff energy in the spectrum should be substantially larger than the ~200 keV/e calculated for the case of Earth. MIMI is ideally suited for making the required measurements of energy spectrum, composition, and anisotropy to test diffusive shock acceleration models.

Another source for upstream particle events is leakage of energetic magnetospheric ions (and electrons) into the interplanetary medium. Observations at Earth,

Jupiter, Saturn, and Uranus have been interpreted as favoring this hypothesis (Krimigis, 1986; 1992). MIMI/INCA and MIMI/CHEMS will measure ion composition and charge state down to ~7 keV/nuc and ~3 keV/e, respectively, unambiguously separating accelerated solar wind ions (high charge states) from ions of magnetospheric origin (low charge states). MIMI/LEMMS will measure the anisotropy of these events at energies above 30 keV.

2.5.4 *MIMI/INCA Remote Sensing of Heliospheric Shocks*

ENAs are produced whenever energetic singly charged ions undergo charge-exchange (electron capture) collisions with a background population of neutral atoms. These conditions occur not only within planetary magnetospheres, but also in the interplanetary medium throughout the heliosphere. The neutral atoms therein are those of the interstellar gas that flows through the heliosphere and thereby generate the pickup ions, discussed in Section 2.5.2. Those ionization processes systematically diminish the density of interstellar neutrals in the inner heliosphere. For hydrogen, the dominant atom, the attenuation is the most severe, setting in at ~3 AU and reducing the H atom intensity to ~95% of the interstellar value by 1 AU. The energetic, singly charged ions, again predominantly hydrogen, are protons accelerated by processes associated with the formation and propagation of heliospheric shocks.

Three types of shocks can accelerate protons to energies >10 keV and thus be imaged in ENA by MIMI/INCA: (1) the forward and reverse shocks produced by corotating interaction regions (CIRs); (2) the driven shocks associated with large solar flare ejecta and coronal mass ejections (CMEs); and (3) the termination shock (TS) of the heliosphere itself, where the supersonic solar wind makes a transition to the subsonic interstellar plasma. Roelof (1992) estimated the ENA intensities >10 keV as they would be viewed by Cassini at Saturn for the first two types of interplanetary shocks, while Hsieh et al. (1992b) provided estimates from 1 AU. A topic of concern in both studies was whether the ENA emission from interplanetary shocks of either type would obscure the ENA emission from the heliospheric termination shock. Hsieh et al. (1992a) had proposed that ENA would be produced at the TS by low-energy anomalous cosmic-ray protons that are eventually accelerated to

~100 MeV. Hilchenbach et al. (1998) claimed to have identified ENA hydrogen at 55-80 keV coming from the anti-apex direction using the CELIAS/HSTOF ion telescope on the SOHO spacecraft during solar minimum conditions.

While the construction of ENA global images of the energetic proton population associated with the heliospheric termination shock is an exciting possibility for MIMI/INCA, the imaging of interplanetary shocks is practically expected. Based on the Voyager 1 and 2 measurements of differential proton intensities j_{ion} for $E > 35$ keV, Roelof (1992) estimated the global distribution of ENA hydrogen intensities as they would be viewed from 10 AU (Saturn orbit) from the general relation

$$j_{\text{ENA}} = \sigma \int \text{ds}\, n_{\text{H}} j_{\text{ion}}.$$

Using Voyager proton spectra representative of the peak values at the shock j_0, (E), the integral intensity (above an energy E) can be written

$$J_{\text{ENA}} = \int \text{d}E\, j_{\text{ENA}} = n_0\, I \int \text{d}E\, \sigma_{16} j_0,$$

where the integral over the spatial dependence of n_{H} and j_{ion} is

$$I = (1.5 \times 10^{-3}\ \text{cm}) \int (\text{ds/a})\, (n_{\text{H}}/n_0)\, (j_{\text{ion}}/j_0).$$

Here σ_{16} is the charge-exchange cross-section in units of 10^{-16} cm^2, a = 1 AU, and $n_0 \cong 0.1$ cm^{-3} is H atom density in the interstellar medium.

Values of the Voyager peak intensity spectra (normalized to 10 AU) and the integral $\int \text{d}E\, \sigma_{16} j_0$ are compiled in Table 2.2, while Figure 2.14 presents the spatial dependence of I as "fish-eye" ENA images of the sunward hemisphere (as viewed

TABLE 2.2

Integral ENA energy coefficient derived from Voyager energetic ions*

E (keV)	10	20	40	70	100	200	400
σ_{16} (cm^2)	7.75	4.45	1.67	0.377	0.101	6.09(−3)	1.76(−4)
j_{ion} (cm^{2}sr s keV)$^{-1}$	[0.70]	[0.55]	0.35	0.20	0.125	0.036	0.010
dE s$_{16}$ j_{ion} (sr s)$^{-1}$	[71.6]	[34.6]	8.81	1.36	0.31	9(−3)	1(−4)

*Ion fluxes in [brackets] are extrapolated downward in energy from 35 keV.

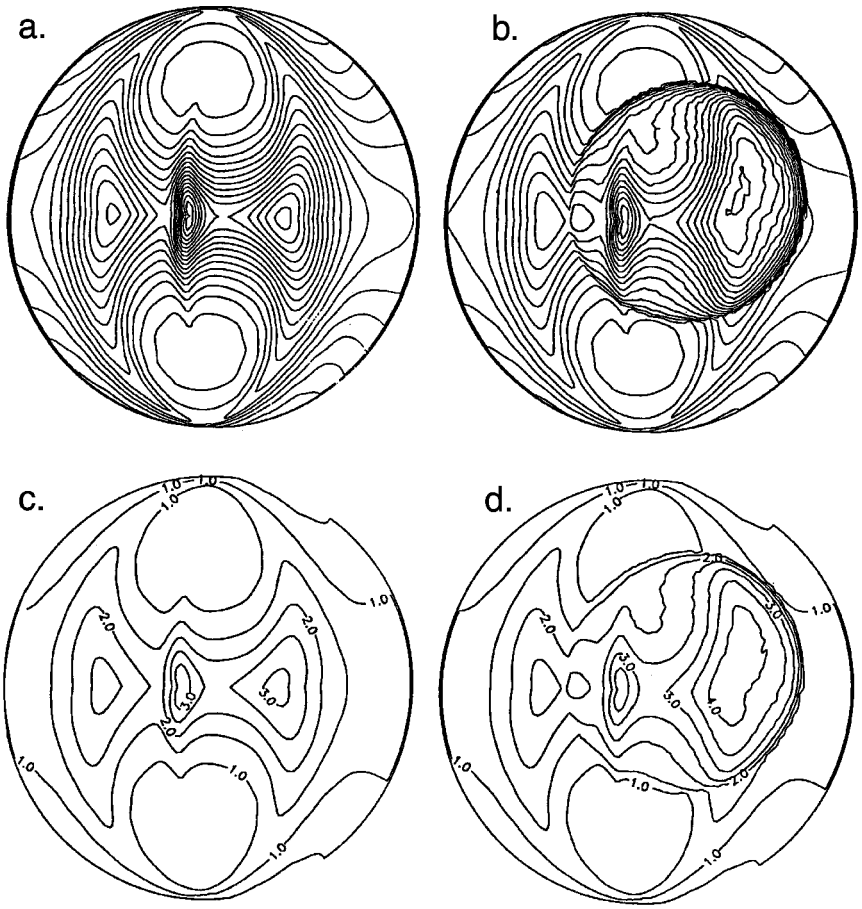

Figure 2.14. Sunward hemisphere views from Saturn (10 AU) of simulated ENA images of interplanetary shock-associated energetic protons from (a) forward and reverse shocks bounding a corotating interaction region (CIR) and (b) solar transient shock superimposed upon a CIR. ENA flux contours are labeled in (c) and (d) in units of 100*I*, as defined in the text, and may be converted into ENA hydrogen flux (as a function of energy) using the values given in Table 2.2.

from Saturn). The ENA images of a large CIR are shown in the left-hand panels, while a large driven shock has been superimposed upon the CIR in the right-hand panels. Contours with $2° \times 2°$ are shown in the upper panels, while a subset of contours of the quantity $100I$ are drawn in the lower panels. The antisunward hemispheres (not shown) exhibit very low contrast, with contours only between 0.5 and 1.0. Based on the instrument response characteristics of MIMI/INCA, Roelof (1992) estimated that images like those shown could be accumulated (in Cassini roll mode)

in 3 days with ~10% counting statistics in 6° × 6° pixels. These statistics were deemed adequate for interpreting the image in terms of global topology, particularly in the portions of the image where the contrast is strongest (at the edge of the shock structure). It was also concluded, in agreement with Hsieh et al. (1992b), that only the largest CIR or transient solar shocks would obscure the ENA emission from protons associated with the global heliospheric shock.